Electrochimica Acta 56 (2011) 1960–1966

Contents lists available at ScienceDirect

Electrochimica Acta

journal homepage: www.elsevier.com/locate/electacta

Enhanced power conversion efficiency in dye-sensitized solar cells with TiO_2 aggregates/nanocrystallites mixed photoelectrodes

Junting Xi[a,b], Qifeng Zhang[a], Kwangsuk Park[a], Yueming Sun[b], Guozhong Cao[a,*]

[a] Department of Materials Science and Engineering, University of Washington, Seattle, WA 98195, USA
[b] School of Chemistry and Chemical Engineering, Southeast University, Nanjing, Jiangsu 211189, China

ARTICLE INFO

Article history:
Received 10 September 2010
Received in revised form
12 November 2010
Accepted 17 November 2010
Available online 25 November 2010

Keywords:
Dye-sensitized solar cells
Mixed photoelectrode
Aggregates
Light scattering
Electron transport

ABSTRACT

Photoelectrodes of mixed microsized TiO_2 aggregates and individually dispersed TiO_2 nanocrystallites with different ratios were fabricated and studied for improved power conversion efficiency in dye-sensitized solar cells (DSCs). TiO_2 aggregates/nanocrystallites composites possess several advantages for high performance of DSCs, including the light scattering by the microsized TiO_2 aggregates and the high surface area of nanocrystallites both in aggregates and individually dispersed. A high power conversion efficiency of 7.59% was achieved with mixed TiO_2 aggregates/nanocrystallites photoelectrode using conventional dye N3, without applying anti-reflection coating, back-scattering layer, or chemical treatment. The electron transport properties of DSCs with mixed photoelectrodes were investigated by electrochemical impedance spectra, and the results showed that such a photoelectrode with mixed aggregates and nanocrystallites possess better connectivity for efficient electron transport.

Published by Elsevier Ltd.

1. Introduction

Dye-sensitized solar cells (DSCs) as third generation photovoltaic devices have attracted significant attention due to their low fabrication cost and relatively high power conversion efficiency (PCE) [1–3]. One of the key elements in DSCs is the mesoporous wide band gap semiconductor photoelectrode, which adsorbed a monolayer of dye molecules onto its large surface to capture the incident photons, and to generate electron–hole pairs [4,5]. The typical photoelectrodes are comprised of TiO_2 nanocrystallites (~20 nm) sensitized by *cis*-dithiocyanatobis(4,4′-dicarboxylic acid-2,2′-bipyridine)ruthenium(II), so-called N3 [6]. Films composed of TiO_2 nanocrystallites present a high surface area to adsorb a sufficient amount of dye molecules [1]. The nanocrystallites films show high transparency and negligible light scattering; the sensitizer N3 lacks the absorption in the near-infrared region and presents relatively low optical extinction coefficient [6,7]. These two drawbacks decrease the light harvesting efficiency (LHE) and, thus, limit the power conversion efficiency. There have been many studies on enhancing the LHE of photoelectrodes by synthesizing new efficient dye sensitizers or adding large particles with sizes in the micrometer or submicrometer scale as light scatterers, resulting in significant advancement in DSCs. For example, K8 and K9 complexes synthesized by using 4,4′-bis(carboxyvinyl)-2,2′-bipyridine as the ligand presented the enhanced spectral response and the increased molar extinction coefficients, which reduced transport losses in TiO_2 electrodes and finally improved the PCE [6,8]. Two typical structures of light scattering have been introduced into photoelectrodes (as schematically illustrated in Fig. 1A and B): (1) a combination structure with large particles as scattering centers incorporated into TiO_2 nanocrystallites and (2) a double-layer structure with a light scattering particle overlayer deposited on a TiO_2 nanocrystallites underlayer [9–17]. It has been demonstrated that these two types of light scattering were all effective and enhanced the optical absorption of the photoelectrodes in DSCs. Light scattering changes the path and/or extends the travelling distance of the incident light in the photoelectrodes, thereby enhances the probability of photons being captured by the adsorbed dye molecules, resulting in an increase in LHE [11,18]. However, the introduction of large sized particles for light scattering decreases the desired specific surface area, and causes the reduction of the amount of dye molecules adsorbed (as shown in Fig. 1A), whereas the incorporation of a light scattering particle overlayer results in an increase in film thickness and loss of photons travelling through electrolyte-filled photoelectrodes, as well as the path lengths of the electrons and the recombination rate, shown in Fig 1B [19]. Both the reduction of the dye amount and the increment in the recombination counteract the light scattering effect and thus limit the further improvement of the conversion efficiency.

* Corresponding author. Tel.: +1 206 616 9084; fax: +1 206 543 3100.
E-mail address: gzcao@u.washington.edu (G. Cao).

0013-4686/$ – see front matter. Published by Elsevier Ltd.
doi:10.1016/j.electacta.2010.11.054

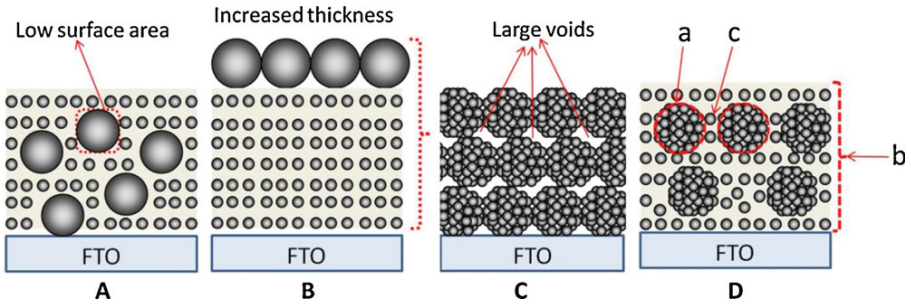

Fig. 1. Schematic of four different types of photoelectrodes with light scatters used in DSCs: (A) nanocrystallites admixed with large particles for light scattering; (B) large particle film was added on top of nanocrystallites film for back scattering; (C) film made of aggregates of nanocrystallites for both high surface area and light scattering; and (D) film with mixed aggregates of nanocrystallites and nanocrystallites for increased surface area per unit area and light scattering.

In recent years, a novel aggregate structure consisting of primary nanocrystallites has been synthesized, providing both large specific surface area and light scattering effect so as to enhance the performance of DSCs [20–22]. Chou et al. [20] first fabricated ZnO film with hierarchical structure consisting of primary nanoparticles ~20 nm in diameter and secondary colloidal spheres ~200–300 nm in diameter, resulting in more photon absorption and electron hole generation, thereby an increase in PCE to ~3.5%, significantly higher than that of DSC with individually dispersed nanocrystallites. Chen et al. [21] synthesized mesoporous TiO_2 beads composed of anatase TiO_2 nanocrystallites to form the photoelectrode, which enhanced the light-harvesting capability without sacrificing the accessible surface for dye loading, resulting in a PCE of 7.2%. Kim et al. [22] designed nanoporous spherical TiO_2 structure for DSCs, providing a novel hierarchical pore structure with high surface area and large pore diameter. Shao et al. [23] synthesized uniform mesoporous TiO_2 nanospheres via an interfacial confined formation process, promoting the dye-loading capacity, electron transfer and light scattering while used in DSCs. The aggregate structure was demonstrated to enhance light scattering and the optical absorption, which was considered as a superior candidate for high performance DSCs. However, large voids between aggregates exist in the photoelectrode films [20,22], as illustrated in Fig. 1C, compared to TiO_2 nanocrystallites films, due to the large sizes of aggregates, which would result in low connectivity for effective charge transfer between aggregates. Such a low connectivity may result in an increased electron diffusion distance and, thus, more charge recombination, leading to a reduced PCE.

The present paper reports the use of a mixture of TiO_2 aggregates and nanocrystallites for the formation of photoelectrode for DSCs, and systematical investigation of the effects of the relative nanocrystallites/aggregates ratio on the performance of DSCs. Fig. 1D shows the schematic microstructure of the mixed aggregates and nanocrystallites used in this study, which highlights three parts: Part a indicates TiO_2 aggregates; Part b shows the film thickness; and Part c is the voids between aggregates within the film. Such a mixed structure is expected to address the drawbacks in the photoelectrodes shown in Fig. 1A–C. Microsized TiO_2 aggregates introduce light scattering without sacrificing the accessible surface area for dye adsorption, and the incorporation of TiO_2 nanocrystallites increases the connectivity for the electron transport, and increases the amount of dye absorbed per unit photoelectrode area without increasing film thickness. A high power conversion efficiency of 7.59% was achieved in a DSC with a photoelectrode consisting of 30 wt% aggregates and 70 wt% TiO_2 nanocrystallites, as compared to 5.80% and 5.35% for DSC with photoelectrodes made of pure nanocrystallites and aggregates, respectively.

2. Experimental

2.1. Preparation and characterization of TiO_2 nanocrystallites and aggregates

TiO_2 nanocrystallites in the anatase phase were obtained by hydrothermally treating TiO_2 sol, as previously described [24]. Microsized TiO_2 aggregates were prepared from an electrospray process [25]. TiO_2 aggregates were electrosprayed from a precursor solution containing of Degussa P25, poly (vinyl pyrrolidone) ($MW \approx 1.3 \times 10^6$), water–ethanol solvent (1:1, v/v) at a flow rate of 0.3 ml/h and an applied voltage of 12 kV. The electrospray setup is the same as which used for electrospinning and has been described in our previous work [25]. The TiO_2 aggregates were collected on aluminum foil and further dried at 100 °C in air for 2 h.

The morphology and surface area of the as-synthesized TiO_2 nanocrystallites and TiO_2 aggregates were characterized by scanning electron microscopy (SEM, JEOL JSM-7000) and Brunauer–Emmett–Teller (BET, Quantachrome NOVA 4200e).

2.2. Preparation and characterization of TiO_2 mixed films

Six pastes containing mixed TiO_2 nanocrystallites and aggregates (labeled as N_1A_0, $N_{0.8}A_{0.2}$, $N_{0.7}A_{0.3}$, $N_{0.6}A_{0.4}$, $N_{0.5}A_{0.5}$, and N_0A_1) were prepared with TiO_2 aggregates concentration of 0, 20, 30, 40, 50, 100 wt%, respectively. The paste was prepared by admixing sample powder with the organic vehicle mainly based on α-terpineol, and then coated on the fluorine-doped tin oxide (FTO) glass substrates as the working electrodes via doctor blade to get approximately 10 μm-thick films [26]. The as-received TiO_2 films underwent a programmed sinter in air as follows: 150 °C for 15 min and at 450 °C for 2 h.

The morphology of mixed films was also characterized by SEM. The optical absorption spectra were measured using an ultraviolet-visible-near infrared (UV–vis-NIR) spectrophotometer (Perkin-Elmer Lambda 900). The mixed films were fabricated on glass substrates with an identical thickness and a blank glass slide was used as a reference during the measurement.

2.3. Device fabrication and characterization

The sintered films were all sensitized by immersing in 0.5 mM ruthenium-based N3 dye solution for 24 h. A Pt-coated silicon substructure was used as the counter electrode, and an iodide-based solution was used as the liquid electrolyte, consisting of 0.6 M tetra-butylammonium iodide, 0.1 M lithium iodide, 0.1 M iodine and 0.5 M 4-tert-butylpyridine in acetonitrile.

To measure the adsorbed N3 dye amount on the mix films, the dye was desorbed by immersing dye-sensitized mixed films

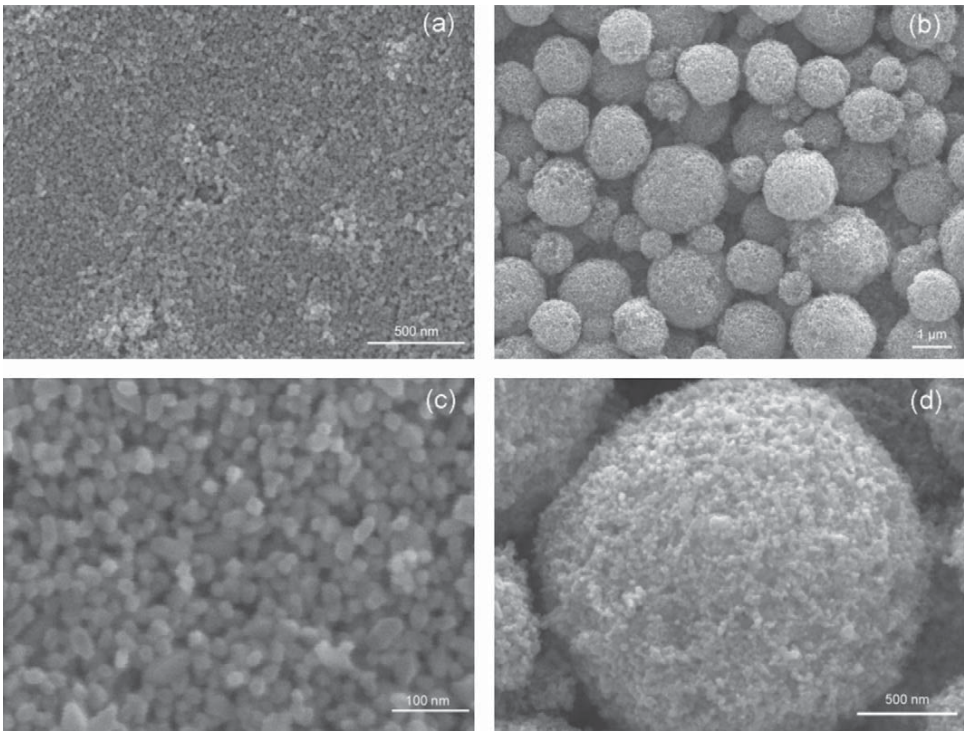

Fig. 2. SEM images of (a) and (c) TiO_2 nanocrystallites film (N_1A_0), and (b) and (d) TiO_2 aggregates film (N_0A_1).

in a 0.1 M NaOH solution in water and ethanol (1:1, v/v). UV–vis-NIR was employed to measure the dye concentration of the desorbed-dye solution. Photovoltaic properties of each solar cell were characterized using simulated AM 1.5 sunlight illumination with an output power of 100 mW/cm^2. An Ultraviolet Solar Simulator (Model 16S, Solar Light Co., Philadelphia, PA) with a 200 W Xenon Lamp Power Supply (Model XPS 200, Solar Light Co., Philadelphia, PA) was used as the light source, and a Semiconductor Parameter Analyzer (4155A, Hewlett-Packard, Japan) was used to measure the current and voltage.

The electrochemical impedance spectroscopy (EIS) was carried out through the Solartron 1287A coupling with the Solartron 1260 FRA/impedance analyzer to investigate electronic and ionic processes in DSCs.

3. Results and discussion

3.1. Morphology and structure of TiO_2 nanocrystallites and aggregates

Fig. 2 shows the scanning electron microscopy (SEM) images of TiO_2 nanocrystallites film (sample N_1A_0) and TiO_2 aggregate film (sample N_0A_1). N_1A_0 is a mesoporous film formed by individually dispersed TiO_2 nanocrystallites of ~20 nm in diameter (seen from Fig. 2c). N_0A_1 comprises the polydisperse spherical aggregates (0.3–2.5 μm in diameter) of P25 TiO_2 nanocrystallites. TiO_2 aggregates were formed by assembling numerous primary ~20 nm-sized P25 TiO_2 nanocrystallites. A rough surface on these aggregates can be observed from Fig. 2d, indicating highly porous nature of the aggregates. Large voids, larger than 1 μm, can be found in the TiO_2 aggregate films (Fig. 2b) compared to much smaller voids, less than 50 nm, in the TiO_2 nanocrystallites films (Fig. 2c).

Fig. 3 shows and compares the typical nitrogen sorption isotherms at 77 K of TiO_2 nanocrystallites and TiO_2 aggregates. The isotherms for both materials showed a type IV pattern with a sharp

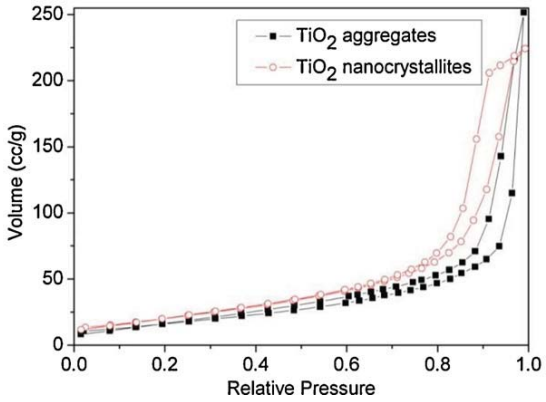

Fig. 3. Nitrogen sorption isotherms of TiO_2 nanocrystallites and TiO_2 aggregates.

inflection of nitrogen adsorbed volume at a high relative pressure (P/P_0 = 0.83–0.95), indicating the nature of mesoporous [16]. The results from BET are detailed in Table 1. The BET surface area in aggregates of P25 TiO_2 nanocrystallites is noticeably lower than that of TiO_2 nanocrystallites that were synthesized in our lab, as Degussa P25 TiO_2 powder has a lower surface area, 52.7 ± 3.6 m^2/g [27], which agrees well with the results obtained in this study and indicates the formation of aggregates had no influence on BET surface area as one would expect. TiO_2 aggregates, however, possess a little higher pore volume than TiO_2 nanocrystallites, which could be

Table 1
BET results for TiO_2 nanocrystallites and TiO_2 aggregates (Degussa P25).

Sample	Surface area (m^2/g)	Pore volume (cm^3/g)
TiO_2 nanocrystallites	82.82	0.346
TiO_2 aggregates (P25)	55.24	0.383

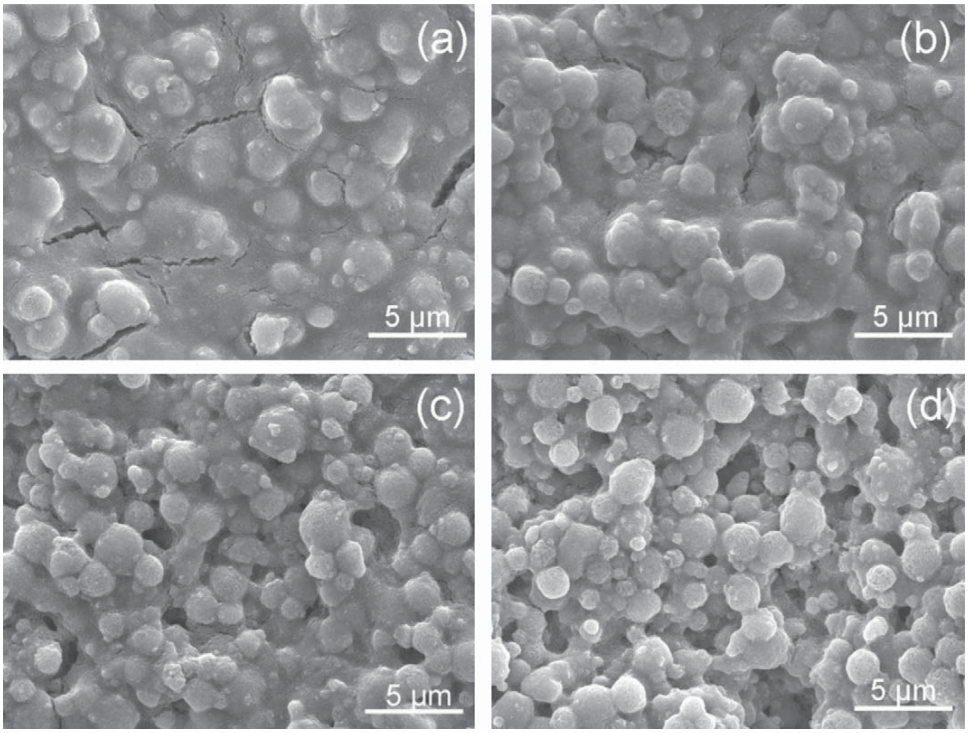

Fig. 4. SEM images of mixed photoelectrodes: (a) $N_{0.8}A_{0.2}$, (b) $N_{0.7}A_{0.3}$, (c) $N_{0.6}A_{0.4}$ and (d) $N_{0.5}A_{0.5}$. In samples $N_{0.8}A_{0.2}$ and $N_{0.7}A_{0.3}$, nanocrystallites have filled up the gaps or voids between microsized aggregates. There remain appreciable voids or gaps in samples $N_{0.6}A_{0.4}$ and $N_{0.5}A_{0.5}$.

attributed to less dense packing of P25 TiO_2 nanocrystallites within the aggregates.

3.2. Morphology and optical absorption of mixed films

Four photoelectrodes consisting of TiO_2 nanocrystallites and aggregates were prepared and referred to as $N_{0.8}A_{0.2}$, $N_{0.7}A_{0.3}$, $N_{0.6}A_{0.4}$, and $N_{0.5}A_{0.5}$ corresponding to respective 20, 30, 40, and 50 wt% ratio of TiO_2 aggregates. Fig. 4 shows the SEM images of photoelectrodes of samples $N_{0.8}A_{0.2}$, $N_{0.7}A_{0.3}$, $N_{0.6}A_{0.4}$ and $N_{0.5}A_{0.5}$. It is observed that sample $N_{0.8}A_{0.2}$ and $N_{0.7}A_{0.3}$ were compact, with TiO_2 aggregates and nanocrystallites mixed homogeneously and there were few large voids in the films (Fig. 4a and b). The large amount of nanocrystallites in the $N_{0.8}A_{0.2}$ film may be responsible for the formation of some cracks. The presence of some large voids was obviously on the films $N_{0.6}A_{0.4}$ and $N_{0.5}A_{0.5}$ with the increased concentration of aggregates.

Fig. 5 shows the nominal optical absorption spectra of samples N_1A_0, $N_{0.8}A_{0.2}$, $N_{0.7}A_{0.3}$, $N_{0.6}A_{0.4}$, $N_{0.5}A_{0.5}$, and N_0A_1, indicating the difference in light-absorption capability of each photoelectrode. The introduction of TiO_2 aggregates leads to an appreciable enhancement in the nominal optical absorption. The intrinsic optical absorption of TiO_2 caused by electron transition from the valence band to the conduction band corresponds to the absorption at the wavelength below 390 nm [28]. The nominal absorption at the wavelength above 390 nm is due to the light scattering effect [14]. The light scattering can extend the distance of light travelled within the films [18]. Such increased travelling distance within the photoelectrodes leads to increase nominal absorption throughout the range of wavelengths analyzed in the present study, which would enhance the probability of photons being captured by the dye molecules after dye sensitization. N_0A_1 photoelectrode comprising of the microsized aggregates only shows the highest intensity of absorption, while N_1A_0 consisting of only individually dispersed nanocrystallites presents the lowest one. The optical absorption of the photoelectrodes gradually increased with an increase of the aggregates/nanocrystallites ratio.

3.3. Dye adsorption behavior of mixed films

Fig. 6 compares the estimated surface area and the amount of dye adsorbed on the photoelectrodes relative to the weight ratio of TiO_2 aggregates/nanocrystallites. The surface area of different samples was estimated based on the specific surface area and the weight ratio of TiO_2 aggregates and nanocrystallites. With

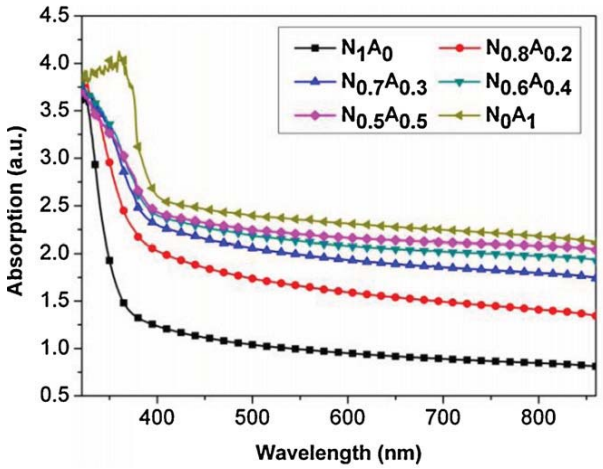

Fig. 5. Nominal optical spectra of the mixed aggregates/nanocrystallites photoelectrodes (N_1A_0, $N_{0.8}A_{0.2}$, $N_{0.7}A_{0.3}$, $N_{0.6}A_{0.4}$, $N_{0.5}A_{0.5}$, and N_0A_1), showing increased nominal optical absorption throughout the entire wavelength studied with increased ratio of aggregates in photoelectrodes.

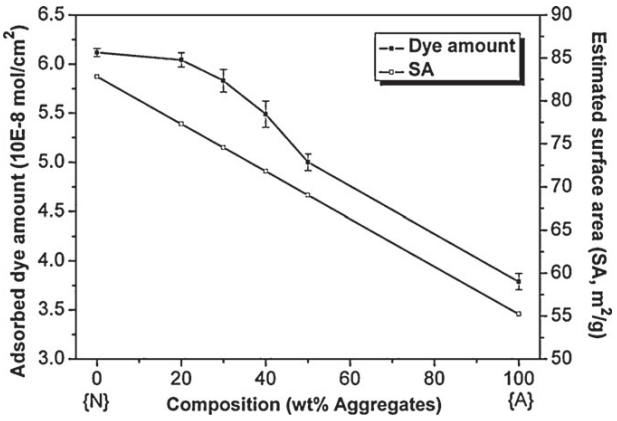

Fig. 6. Comparison of the estimated surface area per unit weight and the amount of dye adsorbed per unit area of photoelectrodes: N_1A_0, $N_{0.8}A_{0.2}$, $N_{0.7}A_{0.3}$, $N_{0.6}A_{0.4}$, $N_{0.5}A_{0.5}$, and N_0A_1.

an increasing concentration of TiO_2 aggregates, the surface area decreases due to the lower BET surface area of aggregates compared to nanocrystallites (shown in Table 1). It was found that the amount of dye adsorbed per unit area of photoelectrodes showed a much less pronounced decrease with an increased concentration of TiO_2 aggregates at the low ratio of aggregates; though a proportional reduction was expected, corresponding to the decreasing surface area. A further increase of aggregate content leads to a reduction of available surface area for dye adsorption. In other words, such experimental results are most likely attributable to the increased available surface areas for dye adsorption, as a result of an increased amount of materials in a given volume (unit area and fixed thickness) in the photoelectrodes. The increased amount of materials in a given volume in photoelectrodes is the reasonable consequence of individually dispersed nanocrystallites filling the large voids between microsized aggregates, as revealed by SEM images (Fig. 4a and b).

3.4. Photovoltaic performance of DSCs with mixed photoelectrodes

Fig. 7a shows the performances or CV curves of DSCs based on photoelectrodes made of N_1A_0, $N_{0.8}A_{0.2}$, $N_{0.7}A_{0.3}$, $N_{0.6}A_{0.4}$, $N_{0.5}A_{0.5}$, and N_0A_1 pastes using N3 as a sensitizer without chemical modification or anti-reflection coating. The open-circuit voltage (V_{oc}), short-circuit current density (J_{sc}), fill factor (FF), and power conversion efficiency (η) of the DSCs are also summarized in Table 2. The DSC with the photoelectrode made of pure TiO_2 aggregates

Table 2
Summary of open-circuit voltage (V_{oc}), short-circuit current density (J_{sc}), fill factor (FF) and power conversion efficiency (η) relative to the mixed photoelectrodes: N_1A_0, $N_{0.8}A_{0.2}$, $N_{0.7}A_{0.3}$, $N_{0.6}A_{0.4}$, $N_{0.5}A_{0.5}$, and N_0A_1.

Photoelectrodes	V_{oc} (V)	J_{sc} (mA/cm^2)	FF	η (%)
N_1A_0	0.81	11.36	0.63	5.80
$N_{0.8}A_{0.2}$	0.78	14.56	0.63	7.15
$N_{0.7}A_{0.3}$	0.78	15.21	0.64	7.59
$N_{0.6}A_{0.4}$	0.80	13.70	0.63	6.90
$N_{0.5}A_{0.5}$	0.80	12.70	0.61	6.20
N_0A_1	0.78	11.06	0.62	5.35

(sample N_0A_1) reached a PCE of 5.35%, whereas that of individually dispersed nanocrystallites (sample N_1A_0) achieved an efficiency of 5.80%. The admixing of TiO_2 aggregates into nanocrystallites led to an obvious improvement on the performance of the DSCs. The remarkably improved power conversion efficiency was attributed mainly to the improvement in J_{sc}, while V_{oc} and FF remained the same. Fig. 7b is a plot of short-circuit current density and PCE as a function of the weight ratio of TiO_2 aggregates/nanocrystallites. With increasing the concentration of TiO_2 aggregates from 0 to 30 wt%, the short-circuit current density and power conversion efficiency increased. When the concentration of aggregates increased further, the short-circuit current density and PCE decreased rapidly.

The maximal PCE achieved in the DSC with photoelectrode made of a mixture of 30 wt% microsized aggregates and 70 wt% individually dispersed nanocrystallites might be explained as the following. Submicron or micron sized aggregates would result in light scattering within the photoelectrodes and, thus, increase the probability of photon capturing, eventually lead to a higher PCE when all other parameters and structures were kept the same [18,19,21]. However, the aggregates introduce significant voids in the resultant photoelectrodes; such large voids result in a loss of less surface area for dye loading in photoelectrodes with given area and thickness. The incorporation of aggregates into nanocrystallites film offers the possibility to maximize the combined optical absorption and dye loading. With increasing the weight ratio of aggregates/nanocrystallites, the optical absorption of the photoelectrodes gradually increased, but at the expense of the amount of dye adsorbed (as shown in Figs. 5 and 6). The opposite but combined impacts of the aggregates/nanocrystallites ratio on the optical absorption and dye loading amount dictate the overall PCE of the DSCs with photoelectrodes made of mixed aggregates and individually dispersed nanocrystallites with varied ratios. The present research reveals that, the optimize weight ratio of aggregates/nanocrystallites was found to be 3:7 for the microsized aggregates and individually dispersed nanocrystallites used in this

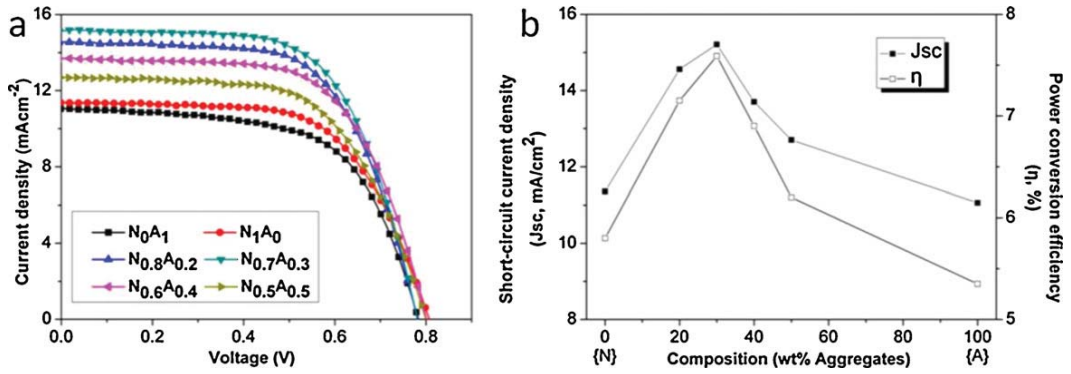

Fig. 7. (a) *I–V* curves of DSCs with mixed photoelectrodes: N_1A_0, $N_{0.8}A_{0.2}$, $N_{0.7}A_{0.3}$, $N_{0.6}A_{0.4}$, $N_{0.5}A_{0.5}$, and N_0A_1; (b) comparison of the short-circuit current density and the power conversion efficiency as a function of the weight ratio of TiO_2 aggregates/nanocrystallites.

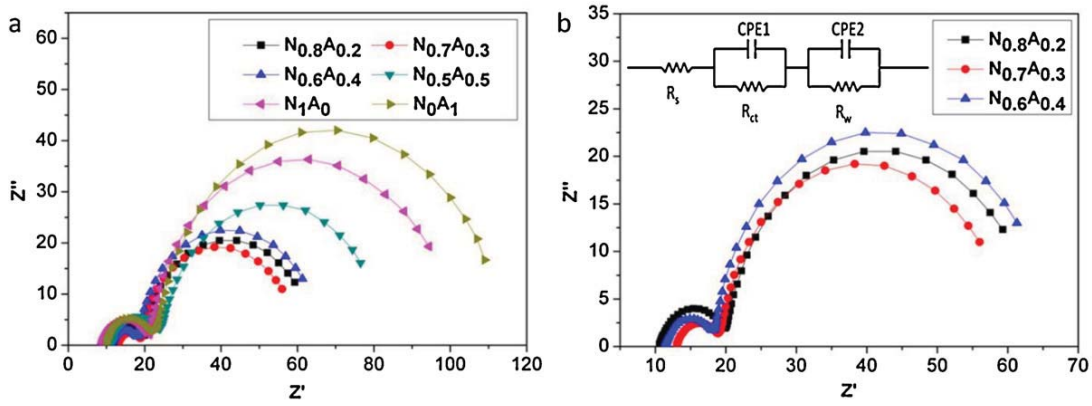

Fig. 8. EIS spectra of DSCs based on mixed photoelectrodes composed of TiO_2 aggregates and nanocrystallites with different weight ratio. (a) Nyquist plots and (b) an enlargement of three plots in the high frequency region of (a). The inset of (b) shows the equivalent circuit of this study.

study, and the highest J_{sc} of 15.21 mA/cm^2 and the highest efficiency of 7.59% were obtained.

3.5. Electron transport properties of DSCs with mixed photoelectrodes

The admixing microsized aggregates with individually dispersed nanocrystallites results in the filling of big voids between aggregates, and thus, offers more surface area for dye adsorption. In addition, such a photoelectrode with mixed aggregates and nanocrystallites is expected to possess better connectivity for efficient charge transport. Electrochemical impedance spectroscopy (EIS) is applied to study the transport properties. Fig. 8a shows the typical EIS Nyquist plots of the DSCs with mixed photoelectrodes composed of different weight ratio of aggregates/nanocrystallites. Fig. 8b presents three plots of sample $N_{0.8}A_{0.2}$, $N_{0.7}A_{0.3}$, and $N_{0.6}A_{0.4}$ with the equivalent circuit inserted. The Nyquist plots exhibit two semicircles including a small semicircle at high-frequency associated with charge transfer resistance at the counter electrode/electrolyte interface and a large semicircle at low-frequency attributed to the electron transport resistance within the TiO_2 films and the charge transfer resistance at the TiO_2/FTO interface and TiO_2/redox electrolyte interface [29–32]. Meanwhile, the equivalent circuit was comprised of a series resistance (R_s), a constant phase element (CPE), an interface charge-transfer resistance (R_{ct}) and a transport resistance (R_w) that combines electron transport resistance and charge transfer resistance [33,34]. Table 3 summarizes and compares the charge transfer resistance R_{ct}, and transport resistance R_w. It is clear that photoelectrodes with both pure nanocrystallites N_1A_0 and pure aggregates N_0A_1 possess much higher transport resistance R_w than that of mixed photoelectrodes. With the amount of aggregates increased from 20 wt% of TiO_2 aggregates ($N_{0.8}A_{0.2}$) to 30 wt% ($N_{0.7}A_{0.3}$), the R_w value decreased from 44.08 Ω to 42.22 Ω. When the amount of aggregates was increased further, these samples presented an increased R_w, for example, R_w increased from 47.67 Ω for $N_{0.6}A_{0.4}$ to 59.13 Ω for $N_{0.5}A_{0.5}$. The R_w represented electron transport resistance within the TiO_2 films and the charge transfer resistance across either TiO_2/FTO interface or TiO_2/redox electrolyte interface. The lower R_w value would result in easier electron transfer within the photoelectrodes [31] and the subsequent charge transfer at photoelectrode/FTO interface [35], which benefit for both electron generation and transport. The EIS results do support the finding that the DSC with photoelectrode made of $N_{0.7}A_{0.3}$ with the lowest R_w offered the highest power conversion efficiency.

Table 3
Summary of charge-transfer resistance (R_{ct}) and transport resistance (R_w) obtained by fitting the impedance spectra of DSCs with mixed photoelectrodes using the equivalent circuit in Fig. 8.

DSC samples	R_{ct} (Ω)	R_w (Ω)
N_1A_0	12.26	79.72
$N_{0.8}A_{0.2}$	9.53	44.08
$N_{0.7}A_{0.3}$	6.32	42.22
$N_{0.6}A_{0.4}$	7.13	47.67
$N_{0.5}A_{0.5}$	13.20	59.13
N_0A_1	13.19	91.03

4. Conclusion

Photoelectrodes with mixed TiO_2 aggregates and TiO_2 nanocrystallites were fabricated and the influences of the aggregates/nanocrystallites ratio on the performance of DSCs were investigated. TiO_2 aggregates with high surface area as scattering centers enhanced light scattering without sacrificing the accessible surface area for dye adsorption, while TiO_2 nanocrystallites filling large voids or gaps between aggregates resulted in the improvement of the dye loading amount per unit area as well as the connectivity for charge transport. The highest power conversion efficiency of 7.59% was achieved with the photoelectrode made of mixed 30 wt% TiO_2 aggregates with 70 wt% nanocrystallites ($N_{0.7}A_{0.3}$), compared to the efficiencies of 5.80% and 5.35% with photoelectrodes made of pure nanocrystallites and pure aggregates, respectively.

Acknowledgements

This work has been supported in part by the US Department of Energy, Office of Basic Energy Sciences, Division of Materials and Engineering under Award no. DE-FG02-07ER46467 (QFZ), National Science Foundation (DMR-1035196), Boeing-Steiner Endowment, University of Washington TGIF grant and Intel Corporation. JTX would also like to acknowledge the fellowship from China Scholarship Council.

References

[1] B. Oregan, M. Gratzel, Nature 353 (1991) 737.
[2] M. Gratzel, Nature 414 (2001) 338.
[3] Q.F. Zhang, C.S. Dandeneau, X.Y. Zhou, G.Z. Cao, Adv. Mater. 21 (2009) 4087.
[4] B. Tan, Y.Y. Wu, J. Phys. Chem. B 110 (2006) 15932.
[5] S. Yodyingyong, Q.F. Zhang, K. Park, C.S. Dandeneau, X.Y. Zhou, D. Triampo, G.Z. Cao, Appl. Phys. Lett. 96 (2010) 3.
[6] M.K. Nazeeruddin, C. Klein, P. Liska, M. Gratzel, Coord. Chem. Rev. 249 (2005) 1460.

[7] M. Gratzel, Inorg. Chem. 44 (2005) 6841.
[8] C. Klein, M.K. Nazeeruddin, P. Liska, D. Di Censo, N. Hirata, E. Palomares, J.R. Durrant, M. Gratzel, Inorg. Chem. 44 (2005) 178.
[9] L. Yang, Y. Lin, J.G. Jia, X.R. Xiao, X.P. Li, X.W. Zhou, J. Power Sources 182 (2008) 370.
[10] L.H. Hu, S.Y. Dai, J. Weng, S.F. Xiao, Y.F. Sui, Y. Huang, S.H. Chen, F.T. Kong, X. Pan, L.Y. Liang, K.J. Wang, J. Phys. Chem. B 111 (2007) 358.
[11] H.J. Koo, J. Park, B. Yoo, K. Yoo, K. Kim, N.G. Park, Inorg. Chim. Acta 361 (2008) 677.
[12] A.G. Agrios, I. Cesar, P. Comte, M.K. Nazeeruddin, M. Gratzel, Chem. Mater. 18 (2006) 5395.
[13] J. Ferber, J. Luther, Sol. Energy Mater. Sol. Cells 54 (1998) 265.
[14] A. Usami, Sol. Energy Mater. Sol. Cells 64 (2000) 73.
[15] G. Rothenberger, P. Comte, M. Gratzel, Sol. Energy Mater. Sol. Cells 58 (1999) 321.
[16] F.Z. Huang, D.H. Chen, X.L. Zhang, R.A. Caruso, Y.B. Cheng, Adv. Funct. Mater. 20 (2010) 1301.
[17] Z.S. Wang, H. Kawauchi, T. Kashima, H. Arakawa, Coord. Chem. Rev. 248 (2004) 1381.
[18] Q.F. Zhang, T.P. Chou, B. Russo, S.A. Jenekhe, G. Cao, Adv. Funct. Mater. 18 (2008) 1654.
[19] Q.F. Zhang, T.R. Chou, B. Russo, S.A. Jenekhe, G.Z. Cao, Angew. Chem. Int. Ed. 47 (2008) 2402.
[20] T.P. Chou, Q.F. Zhang, G.E. Fryxell, G.Z. Cao, Adv. Mater. 19 (2007) 2588.
[21] D.H. Chen, F.Z. Huang, Y.B. Cheng, R.A. Caruso, Adv. Mater. 21 (2009) 2206.
[22] Y.J. Kim, M.H. Lee, H.J. Kim, G. Lim, Y.S. Choi, N.G. Park, K. Kim, W.I. Lee, Adv. Mater. 21 (2009) 3668.
[23] W. Shao, F. Gu, C.Z. Li, M.K. Lu, Inorg. Chem. 49 (2010) 5453.
[24] T.P. Chou, Q.F. Zhang, B. Russo, G.E. Fryxell, G.Z. Cao, J. Phys. Chem. C 111 (2007) 6296.
[25] J.T. Xi, Q.F. Zhang, S.H. Xie, S. Yodyingyong, K. Park, Y.M. Sun, J.Y. Li, G.Z. Cao, Nanosci. Nanotechnol. Lett., submitted.
[26] P. Wang, S.M. Zakeeruddin, J.E. Moser, M. Gratzel, J. Phys. Chem. B 107 (2003) 13280.
[27] T.C. Long, N. Saleh, R.D. Tilton, G.V. Lowry, B. Veronesi, Environ. Sci. Technol. 40 (2006) 4346.
[28] W.G. Yang, F.R. Wan, Y.L. Wang, C.H. Jiang, Appl. Phys. Lett. 95 (2009).
[29] Q. Wang, J.E. Moser, M. Gratzel, J. Phys. Chem. B 109 (2005) 14945.
[30] K.M. Lee, V. Suryanarayanan, J.H. Huang, K.R.J. Thomas, J.T. Lin, K.C. Ho, Electrochim. Acta 54 (2009) 4123.
[31] K. Pan, Y.Z. Dong, C.G. Tian, W. Zhou, G.H. Tian, B.F. Zhao, H.G. Fu, Electrochim. Acta 54 (2009) 7350.
[32] C.P. Hsu, K.M. Lee, J.T.W. Huang, C.Y. Lin, C.H. Lee, L.P. Wang, S.Y. Tsai, K.C. Ho, Electrochim. Acta 53 (2008) 7514.
[33] P.H. Luo, H.J. Niu, G. Zheng, X.D. Bai, M.L. Zhang, W. Wang, Electrochim. Acta 55 (2010) 2697.
[34] H. Xu, X. Tao, D.T. Wang, Y.Z. Zheng, J.F. Chen, Electrochim. Acta 55 (2010) 2280.
[35] Y.T. Shi, C. Zhan, L.D. Wang, B.B. Ma, R. Gao, Y.F. Zhu, Y. Qiu, Adv. Funct. Mater. 20 (2010) 437.